Land-Surface Emissivity Retrieval in MSG–SEVIRI TIR Channels Using MODIS Data

Leonardo F. Peres, Renata Libonati, and Carlos C. DaCamara

Abstract—A procedure is presented that allows using information from the MODerate resolution Imaging Spectroradiometer (MODIS) sensor to improve the quality of emissivity maps for the Meteosat Second Generation/Spinning Enhanced Visible and Infrared Imager (SEVIRI) currently in use as input to a generalized split window (SW) algorithm for land-surface temperature (LST) retrievals in the operational chain of the Satellite Application Facility on Land Surface Analysis (LSA SAF). Information from MODIS is incorporated by means of linear regression models expressing emissivity in SEVIRI thermal-infrared channels as a linear combination of emissivities in MODIS bands. The linear models are applied to the MODIS emissivity product MOD11C3, and a comparison is performed with the operational LSA-SAF product. Special attention is devoted to the semiarid and arid regions of North Africa where emissivity is highly variable. When compared with the new emissivity maps, the LSA-SAF product displays more uniform emissivity values over these regions, leading to higher retrievals for all channels (bias around 0.03) except for IR3.9 (bias from −0.05 to −0.08). The root-mean-square error (RMSE) varies from 0.06 to 0.09 (0.02 to 0.03) for IR3.9 (IR10.8 and IR12.0) and is about 0.06 for IR8.7. The impact on LST is assessed by comparing the retrievals from a SW algorithm using as input the following: 1) the SEVIRI emissivity LSA-SAF product and 2) SEVIRI emissivity maps from MOD11C3. The uncertainty in the LSA-SAF emissivity product results into LST values with bias ranging from −0.4 to −1.0 K and RMSE around 1.6 K. The new emissivity maps based on MODIS data may be an alternative to the standard LSA-SAF emissivity product over semiarid and arid areas, which cover 26% of the land surfaces within the SEVIRI full disk.

Index Terms—Emissivity, land-surface temperature (LST), linear regression, MSG/SEVIRI, TERRA/MODerate resolution Imaging Spectroradiometer (MODIS).

I. INTRODUCTION

THE retrieval of land-surface temperature (LST) from space data is still a challenging task, and most of difficulties encountered are mainly related to the fact that a single radiance measurement is not only affected by LST but also

L. F. Peres is with the Departamento de Meteorologia-Campus Ilha do Fundão-Cidade Universitária, Universidade Federal do Rio de Janeiro, 21949-900 Rio de Janeiro/RJ, Brazil (e-mail: leonardo.peres@igeo.ufrj.br).

R. Libonati is with the Centro de Previsão de Tempo e Estudos Climáticos, Instituto Nacional de Pesquisas Espaciais, 12630-000 Cachoeira Paulista-SP, Brazil.

C. C. DaCamara is with the Centro de Geofísica da Universidade de Lisboa, Instituto Dom Luiz, University of Lisbon, 1749-016 Lisbon, Portugal.

by land-surface emissivity as well as by the thermal structure and composition of the atmosphere. Therefore, any accurate retrieval of LST based on remote sensing measurements requires a proper characterization of the atmospheric influence as well as a net distinction between the effects of LST and emissivity. Even considering the special case of a perfect homogeneous, isothermal, and smooth surface and assuming that the signal has been corrected for all atmospheric influences, a single thermal infrared (TIR) measurement leads to a number of equations that is always less than the number of unknowns. If solely based on observations, the separation of the effects of LST and emissivity is not possible, and therefore, radiative data alone cannot lead to a unique solution of the LST retrieval problem [1]–[3]. One way to close the system of equations is by means of an *a priori* assignment of values of emissivity, and methods commonly used in operational environments, such as the ones based on split window (SW) algorithms (e.g., [4]–[7]), do rely on information extracted from maps of emissivity. In this case, the accuracy of provided emissivity values plays a determinant role on the quality of the retrieved LST.

Because of its simplicity, methods to estimate emissivity using the normalized difference vegetation index (NDVI) have been applied to various sensors providing information on the visible/near infrared [8]. Estimates of emissivity are also usually obtained by combining information on the land cover type as provided by land classifications maps [9]–[11] with laboratory measurements of emissivity as extracted from spectral libraries [12]–[14]. The main advantage of such classification-based emissivity methods is that they offer the possibility of obtaining maps at a global scale. Moreover, no correction of TIR radiance is required, and therefore, no information is required about the atmospheric state. However, when using such type of methods, there is the difficulty of finding a proper way of combining laboratory measurements of emissivity to adequately characterize the different land cover classes [15]. This is especially true when a given surface type (e.g., bare soil) encompasses a large variety of materials, which, in turn, are far from being homogeneous. For instance, satellite observations from the Advanced Spaceborne Thermal Emission and Reflection Radiometer (ASTER) and the MODerate resolution Imaging Spectroradiometer (MODIS) over semiarid and arid regions show significant spatial variability of emissivity associated to the diversity of soils, sands, and rocks; however, land cover maps usually classify such heterogeneous regions as a single surface type, namely, barren, desert, or bare soils [16].

Peres and DaCamara [17] have derived emissivity maps that provide information on emissivity in channels IR3.9, IR8.7, IR10.8, and IR12.0 of the Spinning Enhanced Visible and

Infrared Imager (SEVIRI) on board Meteosat Second Generation (MSG) satellites. The procedure relies on the vegetation cover method [15] where land surface is considered as a heterogeneous system. Catalogued values of emissivity are used to compute emissivity values within SEVIRI channels, and information from the International Geosphere-Biosphere Program (IGBP) land cover map [10] is used to distinguish the different types of land surfaces occurring within the SEVIRI full disk. Proportions of vegetation and ground are then obtained based on information about the fraction of vegetation cover, and an effective emissivity is finally computed. Obtained maps are used for LST retrieval by the generalized SW algorithm [18] that is currently in use in the operational chain of the Satellite Application Facility on Land Surface Analysis (LSA SAF) [19]. Despite its computational efficiency, the ability of the SW algorithm to meet the predefined goal of 2.0 K in LST accuracy [20] crucially depends on the quality of provided maps of emissivity. As expected, problems in the quality of the LSA-SAF LST product have been found over semiarid and arid areas which cover 26% of the land surfaces within the SEVIRI full disk, virtually all corresponding to the Saharan and the Arabian Peninsula regions [17]. Wan *et al.* [21] have pointed out that the classification-based methods used in the 1-km MODIS LST products [14] tend to overestimate emissivity over semiarid and arid regions, leading to an underestimation of LST by the generalized SW algorithm [7]. The quality of the 1-km MODIS LST estimations is poor over these areas, and the usage of LST products based on SW algorithms is especially recommended over lakes, water bodies, snow/ice, and dense vegetated areas where emissivity is well known *a priori*. The retrieval of LST over regions where emissivity is poorly known has, in turn, to rely on methods that do not require *a priori* knowledge of emissivity. In this respect, the validation of LST and emissivity retrievals from MODIS [21] and ASTER data [22] has shown that the MODIS and the ASTER LST/Emissivity products as retrieved respectively by the day/night method [2] and the temperature-emissivity separation (TES) algorithm [3] provide accurate results over semiarid and arid regions because the method ology allows a simultaneous retrieval of LST and emissivity.

Accordingly, the aim of this paper is to discuss how information from other sensors may be used to improve the quality of currently used emissivity maps for SEVIRI over semiarid and arid regions where emissivity is poorly known. We will devote special attention to the MODIS instrument on board TERRA and AQUA satellites and deal with the problem of finding how emissivity in the SEVIRI TIR channels may be optimally expressed by means of linear combinations of emissivities in MODIS bands. For this purpose, different linear regression models are first calibrated using emissivity data from the ASTER spectral library that includes data from three different sources, namely, the John Hopkins University (JHU) Spectral Library, the Jet Propulsion Laboratory (JPL) Spectral Library, and the U.S. Geological Survey (USGS-Reston) Spectral Library [23]. Calibrated models are then validated against emissivity data from the MODIS University of California, Santa Barbara (MODIS-UCSB) Emissivity Library. The obtained optimal linear models are then applied to obtain emissivity maps for SEVIRI channels using, as input, emissivities from

TABLE I
SPECTRAL BANDS IN THE TIR FOR SEVIRI AND MODIS SENSORS

SEVIRI		MODIS	
Channel	CW† (μm)	Channel	CW† (μm)
		20 (3.660-3.840)	3.75
IR3.9 (3.48-4.36)	3.92	22 (3.929-3.989)	3.96
		23 (4.020-4.080)	4.05
IR8.7 (8.3-9.1)	8.70	29 (8.400-8.700)	8.55
IR10.8 (9.80-11.80)	10.80	31 (10.780-11.280)	11.03
IR 12.0 (11.0-13.0)	12.00	32 (11.770-12.270)	12.02
-	-	33 (13.185-13.485)	13.33

†CW stands for Centre Wavelength

the MODIS/TERRA LST/Emissivity Monthly Global 0.05-degree geographic Climate Modeling Grid (CMG) product (MOD11C3). Since the new SEVIRI emissivity maps based on MODIS data will correspond to the MODIS viewing geometry, a semiempirical non-Lambertian model is proposed that allows converting emissivity from MODIS into SEVIRI view angles.

A comparison between the operational SEVIRI LSA-SAF emissivity product and the new SEVIRI emissivity maps based on the MOD11C3 product is performed for January, April, July, and October 2006, and special emphasis is put on the North Africa region where the following conditions are true: 1) emissivity is highly variable; 2) the highest LSA-SAF errors are expected to occur; and 3) the day/night algorithm is expected to allow a proper characterization of emissivity. Finally, the impact on LST is also assessed by comparing the retrievals from a SW algorithm using as input the following: 1) the SEVIRI emissivity LSA-SAF product and 2) SEVIRI emissivity maps from MOD11C3.

II. METHOD AND DATA

The overall procedure consists of the following four steps: 1) preparing data for the calibration and validation of the linear regression models to be developed; 2) calibrating and validating the models; 3) applying the developed models together with retrieved emissivity values from the MODIS sensor to generate maps of land-surface emissivity (LSE) for SEVIRI channels over the MSG disk; and 4) using the new SEVIRI emissivity maps as input to a SW algorithm in order to retrieve LST over the MSG disk.

Table I presents a systematic intercomparison of TIR channels of SEVIRI and MODIS instruments. It may be noted that the MODIS day/night LST algorithm provides estimates of emissivity in seven TIR bands (i.e., channels 20, 22, 23, 29, 31, 32, and 33), all bands but one (i.e., channel 33) lying within the range covered by SEVIRI channels IR3.9, IR8.7, IR10.8, and IR12.0. Taking into account the radiometric resolution and the multiple TIR bands as well as the global coverage provided by the TERRA and AQUA platforms, the MODIS instrument appears as a particularly useful source of information for building up maps of emissivity.

We began by setting up the data sets of channel emissivities for both SEVIRI and MODIS channels covering a wide variety of materials. For this purpose, we have relied on the JHU and the JPL spectral libraries, both included in the ASTER library. We have also used data from the MODIS-UCSB Emissivity Library which were reserved for validation purposes. The
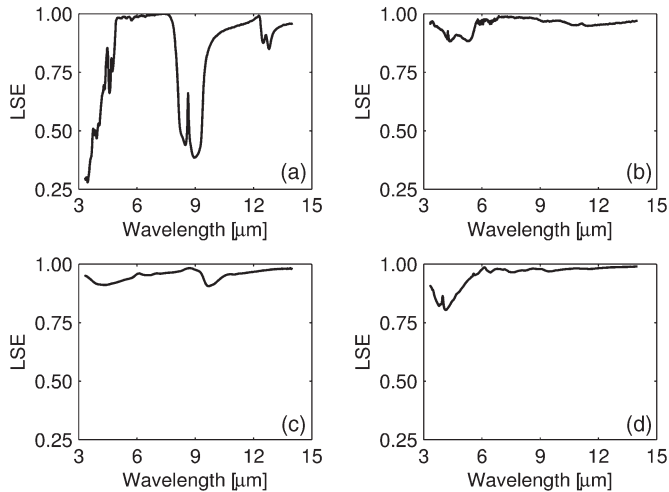
Fig. 1. Spectral emissivity for four different samples, including (a) milk quartz (125–500-μm size range) from JPL, (b) dry grass (sample 1) from MODIS-UCSB, (c) basalt cobble covered with desert varnish provided by John Salisbury, and (d) dark yellowish brown silty clay (aridisol class) from JHU.
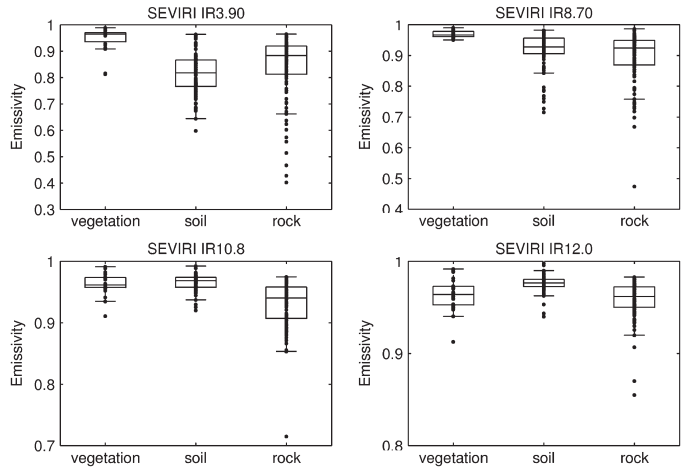

Fig. 2. Emissivity values for SEVIRI channels IR3.9, IR8.7, IR10.8, and IR12.0 with respect to vegetation, soil, and rock classes. Boxes have lines at the lower quartile, median, and upper quartile values. Box whiskers delimit the entire range of the data set.

ASTER library provides a comprehensive collection of over 2300 spectra of a wide variety of materials, including rocks, minerals, lunar soils, terrestrial soils, man-made materials, meteorites, vegetation, snow, and ice, covering the visible through TIR wavelength region (0.4–15.4 μm). Materials were restricted to those belonging to vegetation, water, soil, rocks, and man-made classes because the spectra of those classes were measured in directional hemispherical reflectance (DHR) allowing the derivation of spectral emissivity by means of Kirchhoff's law [24], i.e.,

$$\varepsilon(\lambda, \theta) = 1 - \rho(\lambda, \theta) \qquad (1)$$

where $\varepsilon(\lambda, \theta)$ is the directional emissivity at the wavelength λ and angle θ and $\rho(\lambda, \theta)$ is the corresponding DHR at the same wavelength, for radiation impinging at the same angle.

Dune sands were represented by means of the milk quartz (125–500-μm size range), based on information from the JPL library. Desert surfaces were further characterized using information (kindly provided by J. W. Salisbury) about basalt cobble covered with desert varnish, thick enough to mask the spectral signature of the underlying rock [13]. Spectral emissivity values computed from (1) and obtained from the four aforementioned spectra collections used in this work (i.e., JHU, JPL, John W. Salisbury, and MODIS-UCBS) are shown in Fig. 1 for four representative samples.

Based on the definition of channel emissivity, the spectral emissivity values were then used to evaluate emissivity for the following: 1) SEVIRI channels IR3.9, IR8.7, IR10.9, and IR12.0 and 2) MODIS channels 20, 22, 23, 29, and 31. Accordingly, we have computed the so-called emissivity for a given channel c of a given sensor (i.e., SEVIRI and MODIS), $\varepsilon_{\text{SENSOR}\_c}$, as follows:

$$\varepsilon_{\text{SENSOR}\_c} = \frac{\int\limits_{\lambda=\lambda_1}^{\lambda=\lambda_2} f_c(\lambda)\varepsilon(\lambda,\theta)B(\lambda,T_s)d\lambda}{\int\limits_{\lambda=\lambda_1}^{\lambda=\lambda_2} f_c(\lambda)B(\lambda,T_s)d\lambda} \qquad (2)$$

where SENSOR_c may take the values SEVIRI_c or MODIS_c, $f_c(\lambda)$ is the spectral response function of the considered sensor in channel c, $B(\lambda, T_s)$ refers to the emitted radiance as given by Planck's function for the surface temperature T_s, and λ_1 and λ_2 are respectively the lower and upper limits of the channel spectral range. It may be noted that the assumption of a constant value for T_s (e.g., $T_s = 300.0$ K) does not introduce significant errors since the dependence of emissivity on temperature is usually very small for most surface materials. For instance, different works (e.g., [7] and [25]) have shown that the Planck's function term in (2) may be taken out of the weighting process without introducing significant errors.

Values of $\varepsilon_{\text{SEVIRI}\_c}$ and $\varepsilon_{\text{MODIS}\_c}$ were accordingly estimated for appropriate channels (see Table I) for a calibration set made of 182 samples from the JHU and JPL libraries as well as from data provided by John W. Salisbury. Values of $\varepsilon_{\text{SEVIRI}\_c}$ and $\varepsilon_{\text{MODIS}\_c}$ were also estimated for a validation set made of 134 samples from the MODIS-UCSB Library. Fig. 2 shows the obtained values of $\varepsilon_{\text{SEVIRI}\_c}$ as a box-and-whisker plot for three classes of materials, namely, vegetation, soil, and rock. The boxes have lines at the lower quartile, median, and upper quartile values, and the whiskers extending from each end of the boxes delimit the entire range of the data set. It may be noted that, for most samples, the lowest values of emissivity are found around 3.9 μm, whereas the largest ones occur around 12.0 μm. With respect to emissivity variability, values near 3.9 μm present the largest fluctuations (0.402 to 0.991), followed by 8.7 (0.474 to 0.995), 11.0 (0.715 to 0.996), and 12.0 μm (0.870 to 0.991) spectral bands. In general, obtained results indicate that emissivity values for vegetation are larger and present less variability than that for soils and rocks.

Let us assume that the emissivity in a given SEVIRI TIR channel c, $\varepsilon_{\text{SEVIRI}\_c}$, may be expressed by means of a linear combination of MODIS channel emissivities, i.e.,

$$\varepsilon_{\text{SEVIRI}\_c} = \sum_{\text{MODIS}\_c=1}^{N} a_{\text{MODIS}\_c}\varepsilon_{\text{MODIS}\_c} + b_{\text{MODIS}} \qquad (3)$$

where predictors $\varepsilon_{\text{MODIS}\_c}$ are the MODIS channel emissivities and a_{MODIS_c} and b_{MODIS} are the unknown coefficients of the model, to be estimated by means of a least square regression. The model given by (3) is calibrated using pairs $(\varepsilon_{\text{SEVIRI}\_c}, \varepsilon_{\text{MODIS}\_c})$ as extracted from the aforementioned calibration set of 182 samples. The model is then validated against the validation set of 134 pairs.

Linear models based on (3) allow converting emissivity from MODIS bands to SEVIRI bands. Emissivity maps for SEVIRI channels IR3.9, IR8.7, IR10.8, and IR12.0 within the SEVIRI disk were therefore obtained in this study by applying the calibrated and validated regressions to the MOD11C3 monthly CMG LST/Emissivity product (Collection-4). This product consists of global gridded composites of monthly averaged temperature and emissivity defined at the 0.05° spatial resolution of the CMG. If the daily (MOD11C1) and eight-day (MOD11C2) products may be able to capture fine vegetation changes and surface wetness variations, the monthly (MOD11C3) product presents the advantage of providing LSE data without gaps due to satellite coverage and clouds. The retrieval of MODIS LST/Emissivity is based on the physics-based day/night algorithm [2] that provides emissivity values for seven MODIS bands (20, 22, 23, 29, and 31–33). The validation of the day/night method using MODIS Airborne Simulator data indicates that retrieved values of LST agree with *in situ* measurements within ±1 K in the range of 263–322 K, recommending the use of the method over bare and sparse vegetated areas [21]. The MODIS emissivity products based on the day/night algorithm were also evaluated using ground-based measurements over a semidesert region, and results show that, on average, the emissivity is underestimated by 0.015 [26]. Recent validation efforts further show that the difference between emissivities retrieved using the day/night algorithm and measured in two field campaigns, one in a desert site and another in grassland, was less than 0.0075 in the 10–12.5-μm range [27].

It may be finally noted that the developed linear models allow converting emissivity in MODIS bands to SEVIRI bands, but the resultant emissivity will correspond to the MODIS view angles, not to SEVIRI disk view angles. Snyder *et al.* [28] have measured the spectral, angular emissivity, and bidirectional reflectance of different materials in the 3–14-μm range and concluded that the change in emissivity with angle was small across the entire range for all of the materials except sand. For bare sand, the change was approximately 2% in the 3.7-, 11.0-, and 12.0-μm regions and was as large as 4% in the 8.7-μm region. Emissivity in Advanced Very High Resolution Radiometer (AVHRR) channel 3 (3.75 μm), as retrieved from bidirectional reflectivity over Northern Africa, exhibited strong variations (up to 15%) for large angles [29]. Similar results for sand were obtained in previous angular emissivity studies [30]. The experimental investigation of the angular variation of the infrared emissivity in the TIR (8–14 μm) band revealed a decrease of emissivity with increasing viewing angle, with clay, sand, slime, and gravel showing variations of approximately 1%–3% from 0° to 65° views, whereas a homogeneous grass cover does not show angular dependence [31]. Petitcolin *et al.* [32] have also shown that the angular variation of emissivity at 3.7 μm is small for vegetation, whereas it may be up to 10%

between nadir and 60° view angle for arid and desert areas. In the case of directional emissivity around 11.0 and 12.0 μm, both angular variations are similar, showing a decrease over arid and sandy areas by 3% if the zenithal view angle shifts from 0° to 60°. For vegetation-covered areas, no significant angular variations are observed [33]. In general, the angular variation is more pronounced for bare soils (arid) than for vegetation-covered surfaces, and angular emissivity effects should be considered in case of sand.

A modified semiempirical Minnert model [34] describing the non-Lambertian behavior of the land surface may be used to convert from MODIS into SEVIRI view angles. This model was successfully applied to the bidirectional reflectivity in AVHRR channel 3 [32] as well as in MSG/SEVIRI channel 4 [35]. According to the Minnert model and taking (1) into account, the directional emissivity in SEVIRI bands as obtained from MODIS may be represented by

$$\varepsilon_{\text{SEVIRI}\_c}\left(\theta_{v_{\text{MODIS}}}\right)$$
$$= 1 - \frac{2\pi}{k+1}\rho_{0_{\text{SEVIRI}\_c}}\cos^{k-1}\left(\theta_{v_{\text{MODIS}}}\right) \quad (4)$$

where $\varepsilon_{\text{SEVIRI}\_c}(\theta_{v_{\text{MODIS}}})$ is the directional emissivity in SEVIRI channel c, but corresponding to the MODIS view zenith angle $\theta_{v_{\text{MODIS}}}$, $\rho_{0_{\text{SEVIRI}\_c}}$ is the reflectivity when both the view zenith angle and solar zenith angle equal to zero, and k is a parameter between 0 and 1, the upper limit corresponding to a Lambertian surface. Inverting (4), the reflectivity in SEVIRI channel c to nadir is given by

$$\rho_{0_{\text{SEVIRI}\_c}}$$
$$= \frac{k+1}{2\pi\cos^{k-1}(\theta_{v\text{MODIS}})}\left[1 - \varepsilon_{\text{SEVIRI}\_c}(\theta_{v\text{MODIS}})\right]. \quad (5)$$

Combining (4) for SEVIRI view zenith angle $\theta_{v_{\text{SEVIRI}}}$ and (5), the directional emissivity in SEVIRI channel c at SEVIRI disk view zenith angles can be derived as

$$\varepsilon_{\text{SEVIRI}\_c}\left(\theta_{v_{\text{SEVIRI}}}\right)$$
$$= 1 - \left[\frac{\cos\left(\theta_{v_{\text{SEVIRI}}}\right)}{\cos\left(\theta_{v_{\text{MODIS}}}\right)}\right]^{k-1}\left[1 - \varepsilon_{\text{SEVIRI}\_c}\left(\theta_{v_{\text{MODIS}}}\right)\right]. \quad (6)$$

Depending on the surface type and cover, values of k normally vary between 0.6 and 0.8 and are estimated by regression between modeled and measured reflectances [29], [32], [35]. Assuming a mean value of 0.7 for k and limiting observations for view zenith angles less than 50°, when the surface emissivity is low (e.g., 0.8), there will be a theoretical maximum error of 0.01. A positive linear correlation of k with NDVI was observed [32], and an empirical model correlating k with NDVI may be addressed in the future.

Conversion from MODIS into SEVIRI view angles should be applied with due care when using MODIS LST/Emissivity products based on the composition of different observations. In such cases, both view zenith angle and emissivity information stored in the product are average values from multiple MODIS observations.
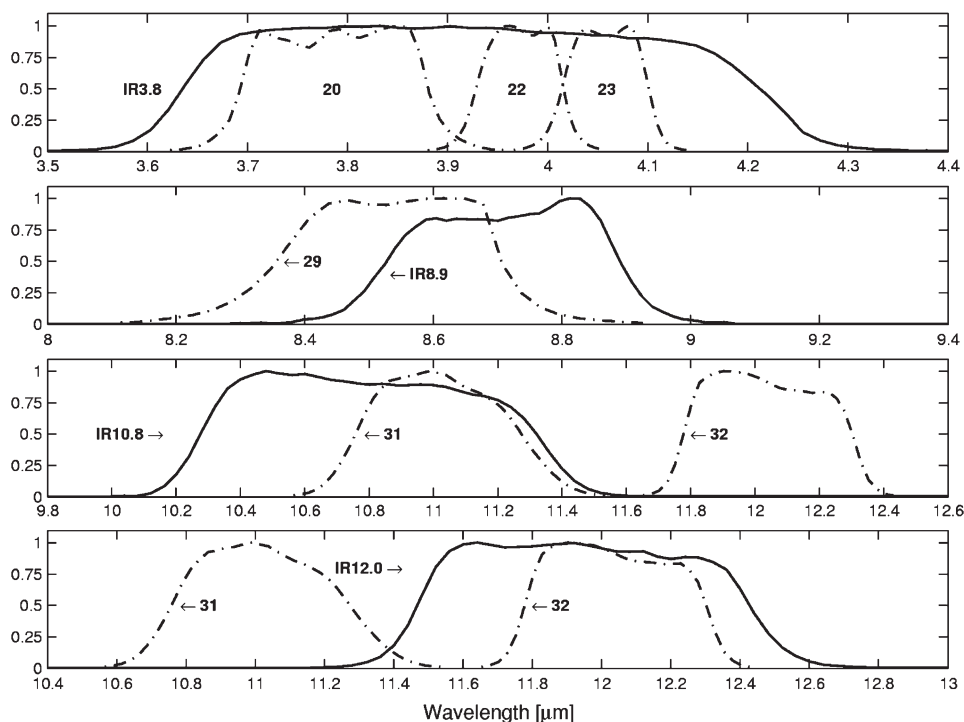
Fig. 3.   Response functions for (solid curve) SEVIRI and (dash-dotted curve) MODIS channels.

TABLE II
QUALITY FIT OF LINEAR MODELS TO ESTIMATE EMISSIVITY IN
SEVIRI CHANNELS BASED ON EMISSIVITY IN MODIS CHANNELS.
LINES IN BOLD IDENTIFY THE CHOSEN LINEAR MODELS

SEVIRI Channel	Used MODIS Channels	RMSE Calib. (Valid.)	R^2_{adj}
IR3.9	20	0.008 (0.007)	0.995
	22	0.026 (0.016)	0.947
	23	0.011 (0.010)	0.990
	20 and 22	0.007 (0.005)	0.996
	20 and 23	**0.003 (0.002)**	**0.999**
	22 and 23	0.011 (0.009)	0.990
	20, 22 and 23	0.003 (0.002)	0.999
IR8.7	**29**	**0.009 (0.009)**	**0.984**
IR10.8	**31**	**0.007 (0.006)**	**0.964**
	31 and 32	0.007 (0.005)	0.964
IR12.0	32	0.002 (0.002)	0.983
	31 and 32	**0.001 (0.002)**	**0.992**

III. RESULTS AND DISCUSSION

A. Calibration and Validation

Fig. 3 presents the response functions of the considered channels of SEVIRI and MODIS instruments. Since SEVIRI bands have broader spectral ranges than MODIS, when building up regression models for a given SEVIRI band, we have analyzed all possible combinations of MODIS channels that are located within that SEVIRI band. As shown in Table II, for each SEVIRI channel, the quality of model fit was assessed by means of the root-mean-square error (RMSE) and the adjusted coefficient of determination (R^2_{adj}). It is worth noting that RMSE was computed in both stages of calibration (i.e., using the data set from JHU) and validation (i.e., using the data set from MODIS-UCSB).

In the case of SEVIRI channel IR3.9, the best results are obtained by combining either MODIS channels 20, 22, and 23,

or just 20 and 23; the latter combination presents the advantage of producing the same level of quality using only two channels. This is either supported by the obtained values of RMSE and R^2_{adj} for calibration and by the obtained values of RMSE for validation.

The linear model for SEVIRI channel IR8.7 relies on MODIS band 29. A value of 0.009 in RMSE was obtained for both calibration and validation.

As shown in Fig. 3, the spectral range of SEVIRI channel IR10.8 contains the whole MODIS band 31 and just covers a very small fraction of band 32. We have therefore tested two linear models, one using just band 31 and the other using bands 31 and 32. Obtained results indicate that adding band 32 does not lead to a significant improvement in the quality of the model fit, and this may be attributed to the small fraction of band 32 that is covered by IR10.8. The good performance of the linear model based on a single channel translates into the obtained value of 0.007 (0.006) of RMSE for calibration (validation).

In the case of SEVIRI channel IR12.0, Fig. 3 clearly shows that the spectral range of IR12.0 entirely covers MODIS band 32 and a fraction of band 31. Unlike in the previous case, the inclusion of MODIS band 31 as a second predictor leads to a decrease in RMSE from 0.002 to 0.001.

In summary, the following linear models were chosen as the most adequate to estimate SEVIRI TIR emissivities from MODIS information:

$$\varepsilon_{\text{SEVIRI\_IR3.9}} = 0.579\varepsilon_{\text{MODIS\_20}}$$
$$+ 0.403\varepsilon_{\text{MODIS\_23}} + 0.017 \quad (7)$$
$$\varepsilon_{\text{SEVIRI\_IR8.7}} = 1.030\varepsilon_{\text{MODIS\_29}} - 0.032 \quad (8)$$
$$\varepsilon_{\text{SEVIRI\_IR10.8}} = 1.023\varepsilon_{\text{MODIS\_31}} - 0.025 \quad (9)$$
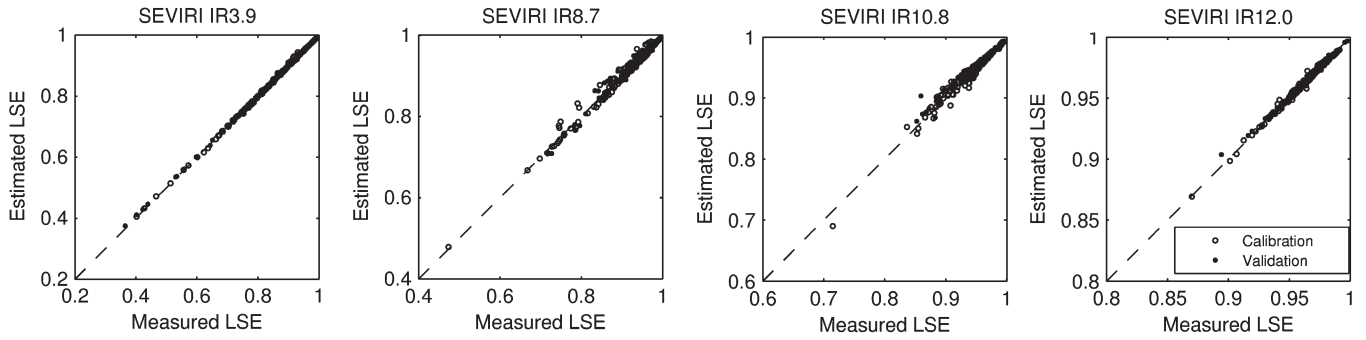
Fig. 4. Measured and predicted values of emissivity in SEVIRI channels IR3.9, IR8.7, IR10.8, and IR12.0 with respect to the linear models given by (7)–(10). White and black circles respectively identify the calibration and validation data sets.
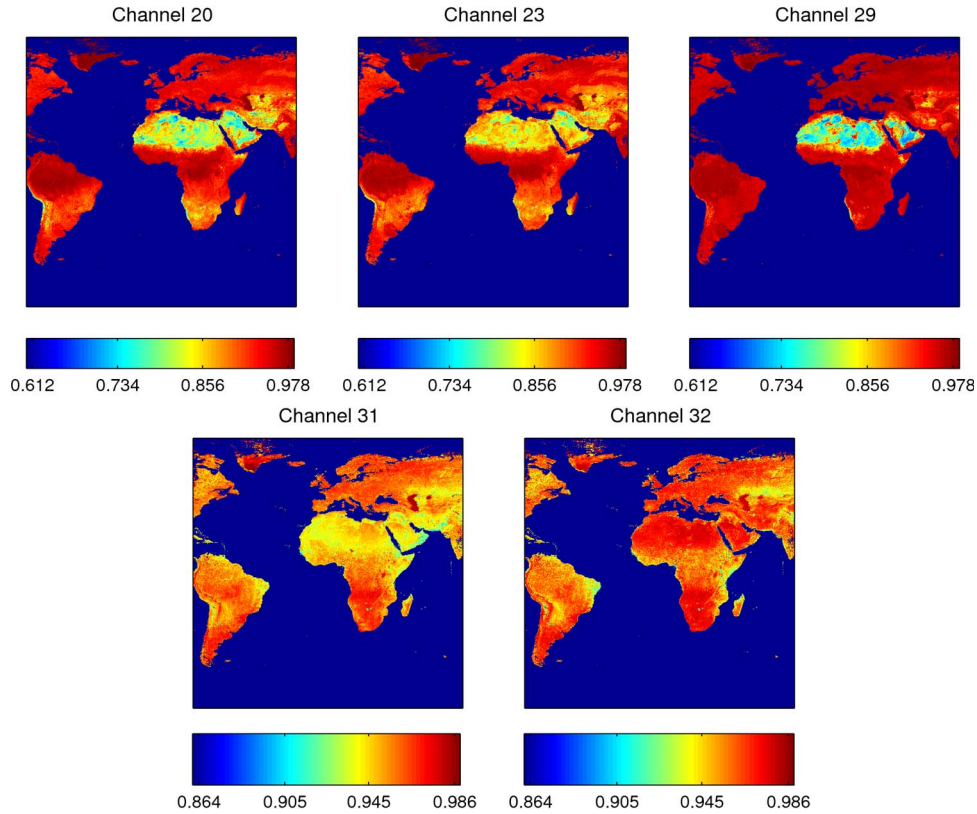

Fig. 5. MOD11C3 Monthly CMG Emissivity Product for July 2006 and with respect to bands 20, 23, 29, 30, 31, and 32.

$$\varepsilon_{\text{SEVIRI\_IR12.0}} = 0.882\varepsilon_{\text{MODIS\_31}}$$
$$+ 0.090\varepsilon_{\text{MODIS\_32}} + 0.027. \quad (10)$$

The adequacy of the chosen models is illustrated in Fig. 4 that presents the measured laboratory emissivity values in SEVIRI channels from ASTER (calibration) and MODIS-UCSB (validation) and the respective predicted values based on MODIS emissivities and from (7)–(10).

B. Comparison With LSA-SAF Emissivity Product

Fig. 5 presents the MOD11C3 monthly CMG LST/LSE product that was used as input data to the linear models. The emissivity fields consist of monthly averages for July 2006 and cover a region from $80°$ S to $80°$ N and from $80°$ W to $80°$ E with a resolution of $0.05° \times 0.05°$. After applying the linear models, the obtained results were reprojected onto the
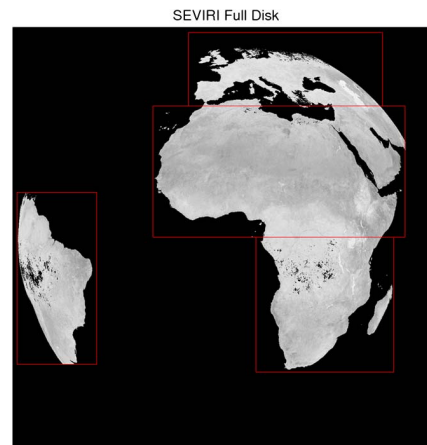

Fig. 6. Limits of the Eur, NAfr, SAfr, and SAme LSA-SAF windows defined within the SEVIRI full disk.
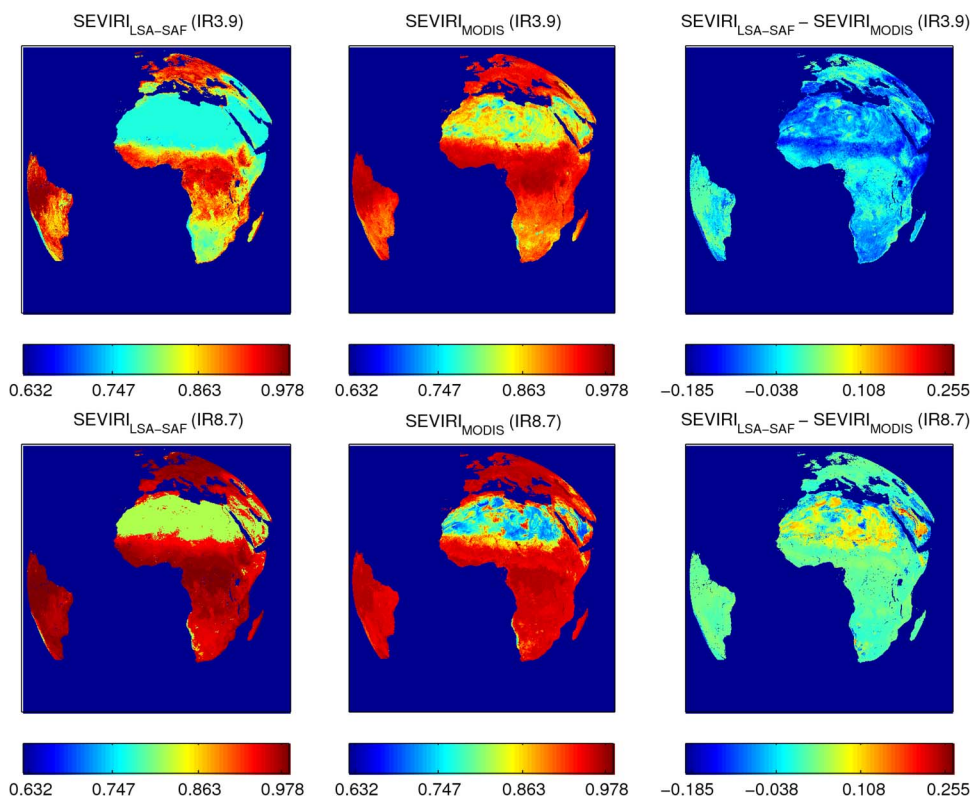
Fig. 7.   LSA-SAF emissivity product and SEVIRI emissivity derived using MOD11C3 product displayed in Fig. 2 and from (7)–(10), and the difference between them over SEVIRI full disk for channels IR3.9 and IR8.7 for July 2006.
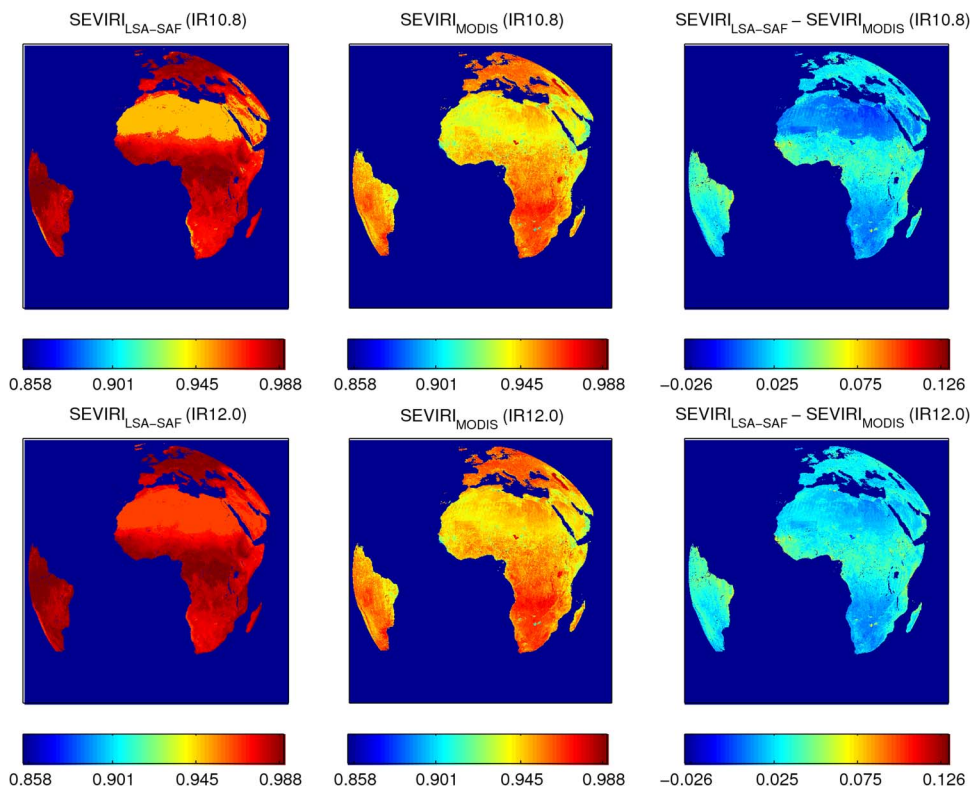

Fig. 8.   As in Fig. 7, but with respect to SEVIRI channels IR10.8 and IR12.0.

so-called normalized geostationary projection (NGP) of MSG [36] using the nearest neighbor resampling method. The projection represents an idealized Earth as viewed from a virtual satellite located over the equator at the nominal longitude of 0°. Since NGP pixels are smaller than those from MOD11C3, original values of LSE are preserved throughout reprojection.

TABLE III
EMISSIVITY MEAN AND STANDARD DEVIATION FOR EACH SEVIRI CHANNEL AND LSA-SAF WINDOW

SEVIRI Channels	LSA-SAF windows			
	Eur	NAfr	SAfr	SAme
IR3.9	0.933 (0.026)	0.884 (0.062)	0.916 (0.035)	0.938 (0.030)
IR8.7	0.959 (0.017)	0.870 (0.087)	0.953 (0.019)	0.957 (0.011)
IR10.8	0.956 (0.009)	0.941 (0.009)	0.958 (0.010)	0.951 (0.010)
IR12.0	0.958 (0.008)	0.946 (0.008)	0.960 (0.010)	0.953 (0.009)

The operational SEVIRI LSA-SAF emissivity product and the results from SEVIRI emissivity maps based on MODIS data were compared taking into account the spatial and spectral consistency of both maps over the four LSA-SAF windows defined within the SEVIRI full disk, namely, Europe (Eur), North Africa (NAfr), South Africa (SAfr), and South America (SAme). The limits of the four windows are shown in Fig. 6. Figs. 7 and 8 present examples of the spatial distribution for July 2006 of the operational SEVIRI LSA-SAF emissivity product and of the derived SEVIRI emissivity from MOD11C3 over the SEVIRI full disk for channels IR3.9, IR8.7, IR10.8, and IR12.0. Both products are quite spatially consistent in channels IR3.9 and IR8.7, except over the Saharan and the Arabian Peninsula regions where Fig. 7 presents uniform emissivity values in the LSA-SAF emissivity product whereas the SEVIRI emissivity maps from MODIS show that emissivity strongly varies in space. The SEVIRI emissivity maps based on MODIS show values that are in agreement with laboratory measurements from ASTER and MODIS-UCSB libraries. Emissivities over densely vegetated areas (e.g., tropical rain forests located in the SAfr and SAme windows) have larger values and show less variability than over dry soils and rocks (e.g., the bare soils located over the Sahara Desert and the Arabian Peninsula in the NAfr window). Table III presents the mean and the standard deviation computed from the SEVIRI emissivity maps based on MODIS for each channel and LSA-SAF window, and it may be noted that results obtained are also consistent with laboratory measurements (see Fig. 2). The lowest mean emissivity values occur in SEVIRI channel IR3.9 for all LSA-SAF windows, except for NAfr that occurs in channel IR8.7 where the mean emissivity (0.870) is slightly lower than that of IR3.9 (0.884). In addition, values of the standard deviation of emissivity in channels IR3.9 and IR8.7 for the NAfr window are also remarkably larger than the variability in the remaining channels. The largest variability occurs in the NAfr window for all channels. The lowest mean emissivity values in IR10.8 and IR12.0 also occur over the NAfr window. This conspicuous spectral behavior of emissivity over NAfr, which is also well apparent in Fig. 7, may be explained by the presence of deserts that may be composed by very different surface types such as regions of sand, exposed bedrock outcrops, and dry soils. The observed heterogeneity is especially pronounced due to the reststrahlen features of silicates, leading to a marked difference between quartz-rich regions and regions that lack silicates. Moreover, the reststrahlen emissivity minima for quartz occur at channel IR8.7 where low emissivity values (around 0.67) can

be observed in the Sahara and Arabian Peninsula, resulting in the lowest mean emissivity (0.870) and the highest standard deviation (0.087). As expected and in agreement with results in Fig. 2, channel IR10.8 systematically presents mean values lower than that of channel IR12.0, and both channels reveal a rather smooth spatial variability over the four windows, with standard deviations varying between 0.008 and 0.010.

The spatial discrepancies between SEVIRI LSA-SAF emissivity product and SEVIRI emissivity maps based on MOD11C3 for channels IR10.8 and IR12.0 shown in Fig. 8 indicate that the inconsistencies are more noticeable in the African continent. The LSA-SAF product presents the maximum emissivity values at Central Africa within Gabon, Republic of the Congo, Democratic Republic of the Congo, and Uganda where the tropical rain forest (broadleaf evergreen) is located. On the other hand, the maximum values in the derived SEVIRI emissivity from MODIS are located at the south part of Central Africa, namely, Angola, and also in part of the Eastern Africa and Southern Africa. The emissivity transition between the Central Africa and the Sahara Desert is also more abrupt in the LSA-SAF product than in the derived SEVIRI emissivity maps where the change is more gradual.

The differences between SEVIRI LSA-SAF emissivity product and SEVIRI emissivity maps based on MOD11C3 were initially assessed based on the bias and RMSE for all pixels within the SEVIRI full disk for July 2006. Results shown in Figs. 7 and 8 indicate that, with the exception of channel IR3.9 (bias around −0.06), the LSA-SAF product overestimates emissivity on the order of 0.02 for all considered channels and, also, that the highest differences are found in channel IR3.9 (RMSE equal to 0.08), followed by IR8.7 (RMSE around 0.05). In the case of channels IR10.8 and IR12.0, the differences have almost the same magnitude, presenting RMSE values around 0.03.

Based on the previous results shown in Figs. 7 and 8 and Table III, a comparison between the operational SEVIRI LSA-SAF emissivity product and the SEVIRI emissivity maps derived using MOD11C3 is also performed focusing on the NAfr window, where emissivity is highly variable and where it is expected, on the one hand, that the highest LSA-SAF errors are located and, on the other hand, that the day/night algorithm allows a proper characterization of emissivity. The poor performance of the LSA-SAF product in the North Africa window is expected and may be explained by taking into consideration that such product presents uniform emissivity values for a large territorial extension (Sahara Desert and Arabian Peninsula). Although the large spatial heterogeneity of emissivity is due
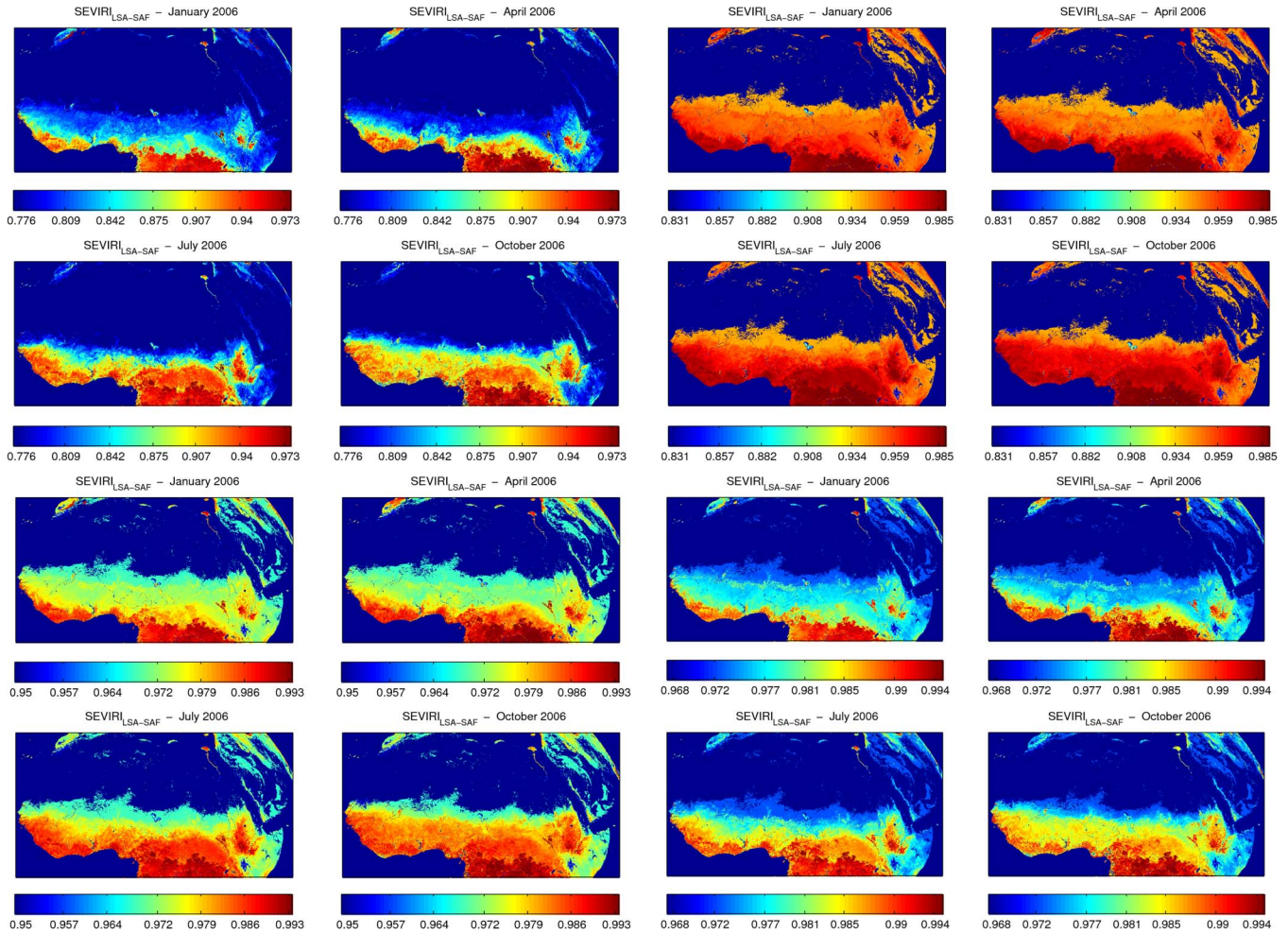
Fig. 9. LSA-SAF emissivity product for SEVIRI channels (upper left panels) IR3.9, (upper right panels) IR8.7, (lower left panels) IR10.8, and (lower right panels) IR12.0 with respect to NAfr window for January, April, July, and October 2006.

to the diversity of soils, sands, and rocks, the IGBP land cover categorizes such areas under a single class, and therefore, the variability among the averaged emissivity values is higher, contributing to the overall product uncertainty in this window.

The operational LSA-SAF emissivity product for SEVIRI channels IR3.9, IR8.7, IR10.8, and IR12.0 with respect to the North Africa window is shown in Fig. 9 for January, April, July, and October 2006, whereas Fig. 10 depicts the obtained SEVIRI emissivity maps from MODIS. The annual variation of the differences between the SEVIRI LSA-SAF product and SEVIRI emissivity from the MOD11C3 product is shown in Fig. 11. Results shown in Table IV confirm that, with the exception of channel IR3.9 (bias varying from -0.05 to -0.08), the LSA-SAF product, in the NAfr window and along the year, tends to have higher values of emissivity (on the order of 0.03) than the product based on MOD11C3. For channel IR3.9 (see Fig. 8) the highest discrepancies occur in January with a bias (RMSE) of -0.08 (0.09), whereas the smallest ones occur in October where the emissivity bias (RMSE) is -0.05 (0.06). In the case of channel IR8.7, July presents the worst agreement with a bias (RMSE) of 0.03 (0.07), whereas the best performance occurs in January where the LSA-SAF product has a bias (RMSE) of 0.02 (0.06). For channels IR10.8 and IR12.0, the LSA-SAF product retrieves emissivity with

bias (RMSE) varying from 0.01 to 0.03 (0.02 to 0.03). Apart from channel IR3.9, the emissivity differences seem to follow the seasonal change in vegetation, with the largest differences occurring during the vegetation growth in spring and summer and the smallest ones during the vegetation decline in fall and winter. For the NAfr window, the worst (best) agreement occurs in April and July (October and January). These results suggest that emissivity differences rise as the vegetation amount starts increasing.

C. Impact on LST

The impact on the LST of the new SEVIRI emissivity maps derived from MOD11C3 was assessed using the following SW algorithm [37], [38]:

$$
\begin{aligned}
T_s = a_0 + a_1 T_{10.8} + a_2(T_{10.8} - T_{12.0}) \\
+ a_3(T_{10.8} - T_{12.0})^2 + a_4(1 - \varepsilon) + a_5 \Delta\varepsilon
\end{aligned}
\tag{11}
$$

where $T_{10.8}$ and $T_{12.0}$ are the brightness temperatures in SEVIRI channels IR10.8 and IR12.0, $\varepsilon = (\varepsilon_{10.8} + \varepsilon_{12.0})/2$ is the average emissivity in SEVIRI channels IR10.8 and IR12.0, $\Delta\varepsilon = (\varepsilon_{10.8} - \varepsilon_{12.0})$ is the emissivity difference between the two channels, and a_k ($k = 0$ to 5) denotes SW coefficients that
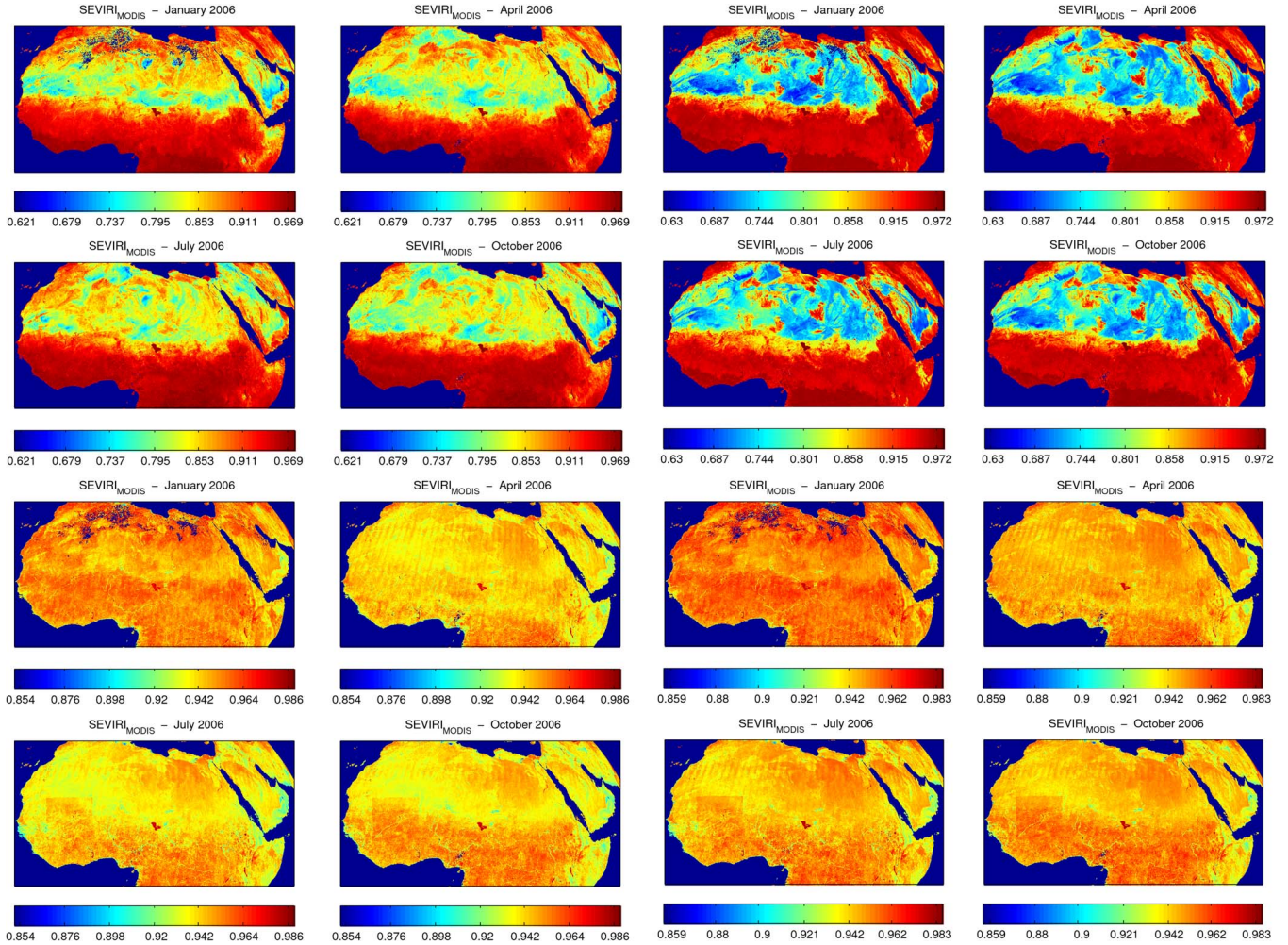
Fig. 10. As in Fig. 9, but with respect to SEVIRI emissivity derived from MOD11C3 product and from (7)–(10).

were estimated by regression analysis using radiative transfer simulations by MODTRAN4 for a wide variety of atmospheric and surface conditions that are likely to be encountered within the MSG disk.

1) *Atmospheric temperature and humidity profiles*: The database relies on atmospheric temperature and humidity profiles from 499 profiles available in the Thermodynamic Initial Guess Retrieval (TIGR3) database. The minimum air temperature at 2 m (the first level), T_a, is 240 K, and the maximum value is 315 K, whereas the water vapor ranges from 0.2 to 6.0 g · cm^{-2}.

2) *LST*: We have considered LST as varying around T_a, from $T_a - 10.0$ K to $T_a + 15.0$ K in steps of 5.0 K.

3) *Land-surface emissivity*: Based on results from [17], ε was considered as varying from 0.90 to 0.99 in steps of 0.01, and $\Delta\varepsilon$ was considered as varying from -0.01 to 0.01 in steps of 0.01.

4) *Satellite zenith angles (SZAs)*: We have selected eight satellite zenith angles covering a range of values from nadir to 60.0°.

In order to obtain an operational SW algorithm, we have also derived a single algorithm that explicitly takes into account the SEVIRI SZA. For this purpose, we have derived a set of new coefficients (b_{0k}, b_{1k}, and b_{2k}) by fitting the SW coefficients a_k to a quadratic function of SZA, as computed for the eight specific SZAs (ranging from nadir to 60°)

$$a_k = b_{0k} + b_{1k}\cos(\text{SZA}) + b_{2k}\cos(\text{SZA})^2. \qquad (12)$$

Finally, a comparison between the LST retrievals obtained with the aforementioned SW algorithm was performed using as input the two following sources of information: 1) SEVIRI LSA-SAF emissivity product, $T_s(\varepsilon_{\text{SEVIRI}})$, and 2) SEVIRI emissivity maps from MOD11C3, $T_s(\varepsilon_{\text{MODIS}})$. MSG observations, performed every 15 min, were selected within the NAfr window on the 15th of January, February, March, and April 2013. The presence of clouds is detected based on the cloud mask (CLM) product from the European Organisation for the Exploitation of Meteorological Satellites (EUMETSAT), which describes the scene type on a pixel level. Each pixel is classified as one of the following four types: clear sky over water, clear sky over land, cloud, or not processed. Results with respect to the spatial distribution of the differences between $T_s(\varepsilon_{\text{SEVIRI}})$ and $T_s(\varepsilon_{\text{MODIS}})$ for 15 UTC are shown in Fig. 12. Table V also shows the bias and RMSE for all pixels within the NAfr and MSG observations along the selected day (96 daily observations). It may be noted that, as shown in Table IV, the LSA-SAF product has higher values of emissivity (from
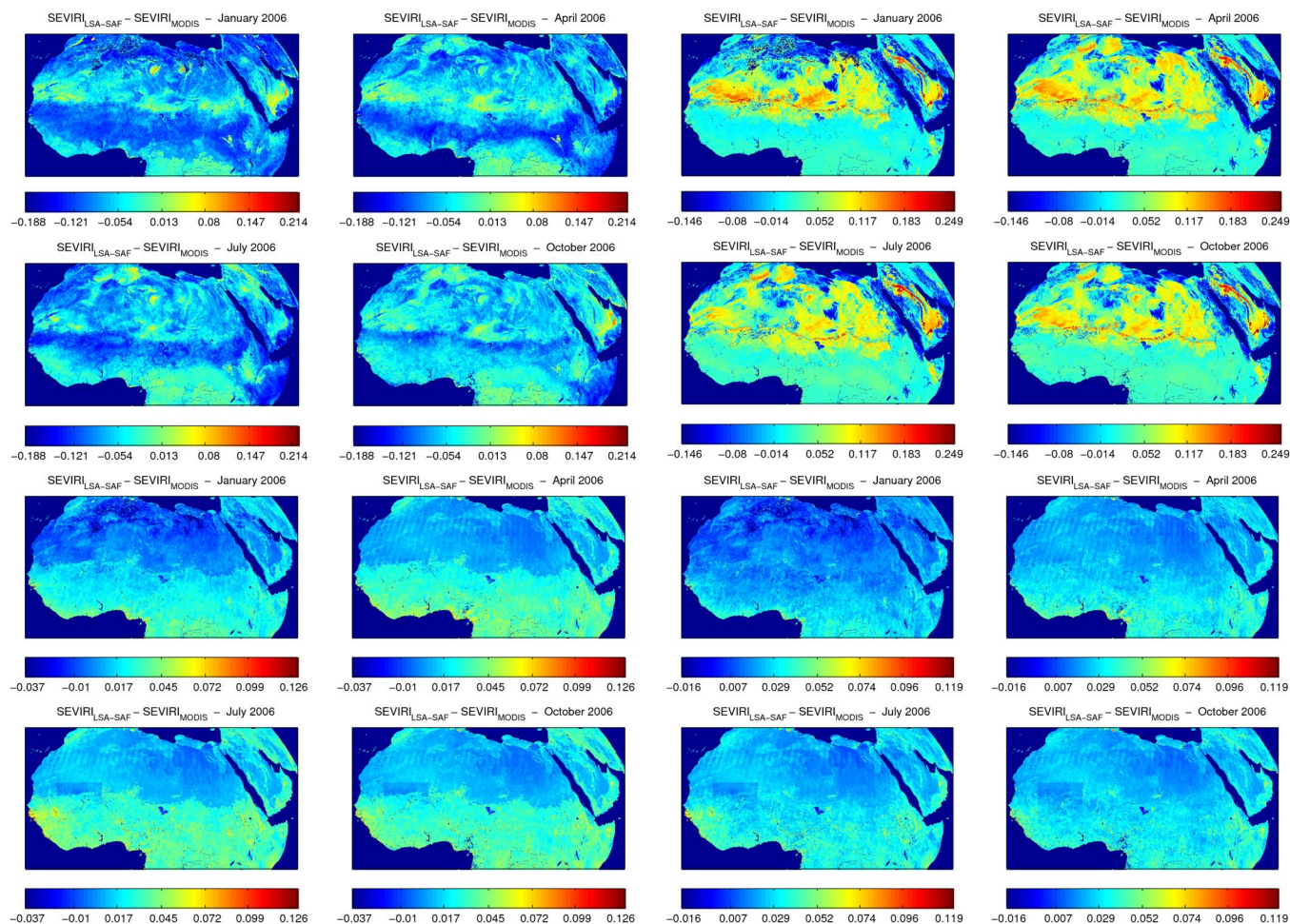
Fig. 11. Difference between SEVIRI LSA-SAF product and SEVIRI emissivity from MOD11C3 product for SEVIRI channels (upper left panels) IR3.9, (upper right panels) IR8.7, (lower left panels) IR10.8, and (lower right panels) IR12.0 with respect to NAfr window for January, April, July, and October 2006.

TABLE IV
BIAS AND RMSE FOR SEVIRI CHANNELS BASED ON THE DIFFERENCE BETWEEN SEVIRI LSA-SAF PRODUCT AND
SEVIRI EMISSIVITY BASED ON MOD11C3 PRODUCT FOR JANUARY, APRIL, JULY, AND NOVEMBER 2006

| Month | SEVIRI Channels | | | | | | | |
| | IR3.9 | | IR8.7 | | IR10.8 | | IR12.0 | |
	Bias	RMSE	Bias	RMSE	Bias	RMSE	Bias	RMSE
1	-0.079	0.090	0.016	0.062	0.012	0.020	0.019	0.021
4	-0.069	0.081	0.030	0.066	0.020	0.025	0.026	0.028
7	-0.079	0.082	0.027	0.063	0.022	0.027	0.028	0.030
10	-0.051	0.064	0.027	0.064	0.020	0.024	0.026	0.028

0.01 to 0.03) in channels IR10.8 and IR12.0 within the NAfr window, leading to lower values of LST by the SW algorithm (ranging from -0.4 to -1.0 K), as shown in Table V. This behavior is nevertheless not observed for all pixels within the NAfr window (see Fig. 12) since the LST retrieved with (11) does vary not only according to the average emissivity in SEVIRI channels IR10.8 and IR12.0 ε but also according to the emissivity difference between the two channels, $\Delta\varepsilon$. The RMSE value around 1.6 K is almost constant during the considered months. Together with the results obtained in Section III-B, the results in this section confirm the determinant

role of emissivity accuracy on the quality of the LST retrievals based on SW algorithms. The total LST error will even be higher since the uncertainties introduced by the atmospheric correction and the instrument noise were not taken into account.

IV. CONCLUSION

Different regression models were built up that allow expressing emissivity in SEVIRI channels IR3.9, IR18.7, IR10.8, and IR12.0 as a linear combination of values of emissivity as derived from MODIS data. The different linear regressions
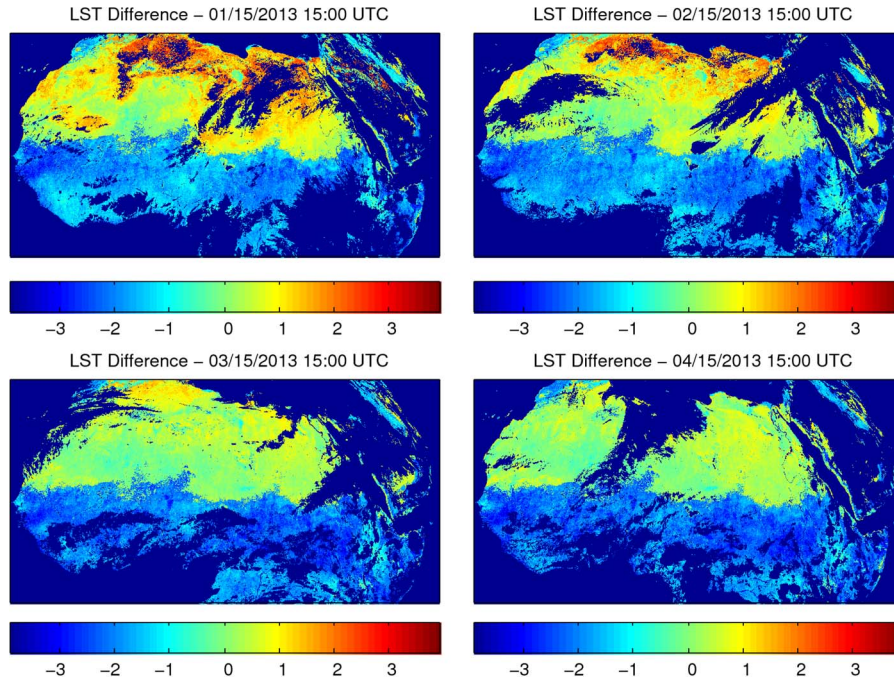
Fig. 12.   Difference between LST retrieved using the SEVIRI LSA-SAF emissivity product and the SEVIRI emissivity maps from MOD11C3 within the NAfr window for the 15th day of January, February, March, and April 2013 at 15 UTC.

TABLE V
BIAS AND RMSE FOR ALL PIXELS WITHIN THE NAfr WINDOW AND
THE 96 MSG OBSERVATIONS ALONG THE SELECTED DAY BASED
ON THE DIFFERENCE BETWEEN LST RETRIEVED USING THE
SEVIRI LSA-SAF EMISSIVITY PRODUCT AND THE
SEVIRI EMISSIVITY MAPS FROM MOD11C3

Date	Bias (K)	RMSE (K)
15/01/2013	-0.40	1.61
15/02/2013	-0.68	1.62
15/03/2013	-0.74	1.60
15/04/2013	-1.00	1.65

were calibrated using 182 samples from JHU and JPL spectral libraries and from data provided by John W. Salisbury. The models were validated against 134 samples from the MODIS-UCSB Emissivity Library. The quality of model fit was assessed by means of the adjusted coefficient of determination and RMSE in both stages of calibration and validation. The values of RMSE are less than 0.01 for the most suitable equations. It may be noted that this value does not take into account errors that are inherent to the MODIS products, which may vary from 0.0075 to 0.015 over bare and sparse vegetated areas when emissivity is evaluated using the day/night algorithm [27].

The calibrated linear models were applied to the MOD11C3 product, which were then reprojected onto the SEVIRI full disk. The MOD11C3 product is retrieved using the day/night method that allows a simultaneous retrieval of LST and emissivity. The choice of the product was due to the fact that MOD11C3 is capable of providing accurate results in semiarid and arid regions where the LSA-SAF emissivity product has revealed poor accuracy due to the difficulty in combining laboratory

emissivity measurements to characterize barren, desert, or bare soil surface types in classification maps.

The operational SEVIRI LSA-SAF product and the new emissivity product based on MODIS data were compared taking into account the spatial and spectral consistency of both maps over the SEVIRI full disk. Results over the NAfr window indicate that, with the exception of channel IR3.9 (bias varying from -0.05 to -0.08), the operational LSA-SAF product presents higher values of emissivity along the year with a bias of about 0.03. RMSE varies from 0.06 to 0.09 for IR3.9 and is about 0.06 for IR8.7, whereas for channels IR10.8 and IR12.0, emissivity is retrieved with RMSE varying from 0.02 to 0.03. The impact of the new emissivity maps on LST was also assessed taking into account the differences between LST retrievals based on LSA-SAF emissivity product and emissivity maps from MOD11C3. The uncertainty in the LSE values from the standard LSA-SAF emissivity product when used as input to a SW algorithm may lead to LST values with bias ranging from -0.4 K to -1.0 K and RMSE around 1.6 K. The total LST error is expected to be even higher due to the error from the atmospheric correction and the instrument performance. Accordingly, for surface and atmospheric conditions where the LST goal accuracy of 2.0 K is not achieved by using the LSA-SAF emissivity product, the new improved emissivity maps based on MOD11C3 may be alternatively used, namely, over semiarid and arid areas, which cover 26% of the land surfaces within the SEVIRI full disk.

The validation of the operational LSA-SAF emissivity product by means of comparisons between data retrieved from satellite and from *in situ* point measurements has proven to be especially challenging [38], [39]. The major problem relates with the scale mismatch between ground point measurements (3 to 50 cm) and the SEVIRI resolution (of about 5 km). The

approach proposed in this paper may partially circumvent this problem since it may be used to compare emissivity products as derived from different satellite data and the respective impacts that are to be expected on the retrieval of LST. For instance, the linear models based on (3) may be applied using as input a variety of available MODIS products, namely, the new MODIS-TES (MOD21_L2) product developed at JPL using the TES algorithm [40]. Similar linear regression models as those proposed here may also be developed and applied for other in-orbit sensors (e.g., the NOAA AVHRR and the Geostationary Operational Environmental (GOES) Imager).

By allowing a proper comparison between the LSA SAF and the suite of MODIS emissivity products, linear regression models such as those developed in this paper may be used to assess the overall consistency of emissivity maps, particularly those operationally used by the LSA SAF. The procedure will also allow assessing the performance of different emissivity–temperature separation methods that have been developed to estimate emissivity from MSG/SEVIRI, namely, the two-temperature method [1], the hybrid method [38], [39], and the temperature-independent spectral index method [35], [41]. When using such methods, SEVIRI emissivity maps derived from MODIS data may be further used to define more reliable ranges of admissible solutions, leading to the definition of narrower constraints in the space of solutions and, therefore, to more reliable estimates of emissivity and LST.

REFERENCES

[1] L. F. Peres and C. C. DaCamara, "LST and emissivity estimation based on the two-temperature method: Sensitivity analysis using simulated MSG/SEVIRI data," *Remote Sens. Environ.*, vol. 91, no. 3/4, pp. 377–389, Jun. 2004.

[2] Z. Wan and Z.-L. Li, "A physical-based algorithm for land-surface emissivity and temperature from EOS/MODIS data," *IEEE Trans. Geosci. Remote Sens.*, vol. 35, no. 4, pp. 980–996, Jul. 1997.

[3] A. Gillespie, S. Rokugawa, T. Matsunaga, J. S. Cothern, S. Hook, and A. B. Kahle, "A temperature and emissivity separation algorithm for advanced spaceborne thermal emission and reflection radiometer (ASTER) images," *IEEE Trans. Geosci. Remote Sens.*, vol. 36, no. 4, pp. 1113–1126, Jul. 1998.

[4] J. C. Price, "Land surface temperature measurements from the split window channels of the NOAA-AVHRR," *J. Geophys. Res.*, vol. 89, no. D5, pp. 7231–7237, Aug. 1984.

[5] F. Becker and Z.-L. Li, "Toward a local split window method over land surface," *Int. J. Remote Sens.*, vol. 11, no. 3, pp. 369–393, 1990.

[6] J. A. Sobrino, C. Coll, and V. Caselles, "Atmospheric corrections for land surface temperature using AVHRR channel 4 and 5," *Remote Sens. Environ.*, vol. 38, no. 1, pp. 19–34, Oct. 1991.

[7] Z. Wan and J. Dozier, "A generalised split-window algorithm for retrieving land-surface temperature from space," *IEEE Trans. Geosci. Remote Sens.*, vol. 34, no. 4, pp. 892–905, Jul. 1996.

[8] A. A. Van de Griend and M. Owe, "On the relationship between thermal emissivity and the normalized difference vegetation index for natural surfaces," *Int. J. Remote Sens.*, vol. 14, no. 6, pp. 1119–1131, Apr. 1993.

[9] A. S. Belward and T. Loveland, "The IGBP-DIS 1 km land cover project, remote sensing in action," in *Proc. 21st Annu. Conf. Remote Sens. Soc.*, Southampton, U.K., Sep. 11–14, 1995, pp. 1099–1106.

[10] T. R. Loveland, B. C. Reed, J. F. Brown, D. O. Ohlen, J. Zhu, L. Yang, and J. W. Merchant, "Development of a global land cover characteristics database and IGBP DIScover from 1-km AVHRR data," *Int. J. Remote Sens.*, vol. 21, no. 6/7, pp. 1303–1330, Apr. 2000.

[11] M. A. Friedl, D. K. McIver, J. C. F. Hodges, X. Zhang, D. Muchoney, A. H. Strahler, C. E. Woodcock, S. Gopal, A. Schnieder, A. Cooper, A. Baccini, F. Gao, and C. Schaaf, "Global land cover from MODIS: Algorithms and early results," *Remote Sens. Environ.*, vol. 83, no. 1/2, pp. 287–302, Nov. 2002.

[12] J. W. Salisbury and D. M. D'Aria, "Emissivity of terrestrial materials in the 8–14 μm atmospheric window," *Remote Sens. Environ.*, vol. 42, no. 2, pp. 83–106, Nov. 1992.

[13] J. W. Salisbury and D. M. D'Aria, "Emissivity of terrestrial materials in the 3–5 μm atmospheric window," *Remote Sens. Environ.*, vol. 47, no. 3, pp. 345–361, Mar. 1994.

[14] W. C. Snyder, Z. Wan, Y. Zhang, and Y.-Z. Feng, "Classification-based emissivity for land surface temperature measurement from space," *Int. J. Remote Sens.*, vol. 19, no. 14, pp. 2753–2774, 1998.

[15] V. Caselles and J. A. Sobrino, "Determination of frosts in orange groves from NOAA-9 AVHRR data," *Remote Sens. Environ.*, vol. 29, pp. 135–146, Sep. 1989.

[16] K. Ogawa, T. Schmugge, and F. Jacob, "Estimation of land surface window (8–12 μm) emissivity from multi-spectral thermal infrared remote sensing—A case study in a part of Sahara Desert," *Geophys. Res. Lett.*, vol. 30, no. 2, pp. 39-1–39-4, Jan. 2003.

[17] L. F. Peres and C. C. DaCamara, "Emissivity maps to retrieve land-surface temperature from MSG/SEVIRI," *IEEE Trans. Geosci. Remote Sens.*, vol. 45, no. 8, pp. 1834–1844, Aug. 2005.

[18] I. F. Trigo, I. T. Monteiro, F. Olesen, and E. Kabsch, "An assessment of remotely sensed land surface temperature," *J. Geophys. Res.*, vol. 113, no. D17, pp. D17108-1–D17108-12, Sep. 2008.

[19] I. F. Trigo, C. C. DaCamara, P. Viterbo, J.-L. Roujean, F. Olesen, C. Barroso, F. Camacho-de Coca, S. C. Freitas, J. García-Haro, B. Geiger, F. Gellens-Meulenberghs, J. Meliá, L. Pessanha, and N. Siljamo, "The satellite application facility for land surface analysis," *Int. J. Remote Sens.*, vol. 32, no. 10, pp. 2725–2744, May 2011.

[20] *User Requirement Document. EUMETSAT Internal Documentation*, LSA-SAF Team, 2003, Doc. No. SAF/LAND/URD/6.2, Issue: Version 6.2.

[21] Z. Wan, Y. Zhang, Q. Zhang, and Z.-L. Li, "Validation of the land-surface temperature products retrieved from Terra Moderate Resolution Imaging Spectroradiometer data," *Remote Sens. Environ.*, vol. 83, no. 1/2, pp. 163–180, Nov. 2002.

[22] F. Jacob, F. Petitcolin, T. Schmugge, E. Vermote, A. French, and K. Ogawa, "Comparison of land surface emissivity and radiometric temperature derived from MODIS and ASTER sensors," *Remote Sens. Environ.*, vol. 90, no. 2, pp. 137–152, Mar. 2004.

[23] A. M. Baldridge, S. J. Hook, S. I. Grove, and G. Rivera, "The ASTER spectral library version 2.0," *Remote Sens. Environ.*, vol. 113, pp. 711–715, 2009.

[24] J. W. Salisbury, A. Wald, and D. M. D'Aria, "Thermal-infrared remote sensing and Kirchhoff's law 1. Laboratory measurements," *J. Geophys. Res.*, vol. 99, no. B6, pp. 11897–11911, Jun. 1994.

[25] A. C. Wilber, D. P. Kratz, and S. K. Gupta, "Surface Emissivity Maps for Use in Satellite Retrievals of Longwave Radiation," NASA Langley Research Center, Hampton, VA, USA, Tech. Rep. NASA/TP-1999-209362, 1999.

[26] K. Wang, Z. Wan, P. Wang, M. Sparrow, J. Liu, and S. Haginoya, "Evaluation and improvement of the MODIS land surface temperature/emissivity products using ground-based measurements at a semi-desert site on the western Tibetan Plateau," *Int. J. Remote Sens.*, vol. 28, no. 11, pp. 2549–2565, Jan. 2007.

[27] Z. Wan, "New refinements and validation of the MODIS land-surface temperature/emissivity products," *Remote Sens. Environ.*, vol. 112, no. 1, pp. 59–74, Jan. 2008.

[28] W. C. Snyder, Z. Wan, Y. Zhang, and Y. Feng, "Thermal infrared (3–14 μm) bidirectional reflectance measurements of sand and soils," *Remote Sens. Environ.*, vol. 60, no. 1, pp. 101–109, Apr. 1997.

[29] F. Nerry, F. Petitcolin, and M. P. Stoll, "Bidirectional reflectivity in AVHRR channel 3: Application to a region in Northern Africa," *Remote Sens. Environ.*, vol. 66, no. 3, pp. 298–316, Dec. 1998.

[30] Y. Takashima and K. Masuda, "Emissivities of quartz and Sahara dust-powers in the infrared region (7–17 μm)," *Remote Sens. Environ.*, vol. 23, no. 1, pp. 51–63, Oct. 1987.

[31] J. A. Sobrino and J. Cuenca, "Angular variation of thermal infrared emissivity for some natural surfaces from experimental measurements," *Appl. Opt.*, vol. 38, no. 18, pp. 3931–3936, Jun. 1999.

[32] F. Petitcolin, F. Nerry, and M. P. Stoll, "Mapping directional emissivity at 3.7 μm using a simple model of bi-directional reflectivity," *Int. J. Remote Sens.*, vol. 23, no. 17, pp. 3443–3472, Sep. 2002.

[33] F. Petitcolin, F. Nerry, and M. P. Stoll, "Mapping temperature independent spectral indice of emissivity and directional emissivity in AVHRR channels 4 and 5," *Int. J. Remote Sens.*, vol. 23, no. 17, pp. 3473–3491, Sep. 2002.

[34] M. Minnaert, "The reciprocity principle of lunar photometry," *Astrophys. J.*, vol. 93, pp. 403–410, May 1941.

[35] G.-M. Jiang, Z.-L. Li, and F. Nerry, "Land surface emissivity retrieval from combined mid-infrared and thermal infrared data of MSG-SEVIRI," *Remote Sens. Environ.*, vol. 105, no. 4, pp. 326–340, Dec. 2006.

[36] *LRIT/HRIT Global Specification*, Coordination Group for Meteorological Satellites, Darmstadt, Germany, 1999, Issue 2.6.

[37] J. A. Sobrino and N. Raissouni, "Toward remote sensing methods for land cover dynamic monitoring: Application to Morocco," *Int. J. Remote Sens.*, vol. 21, no. 2, pp. 353–366, Jan. 2000.

[38] L. F. Peres, J. A. Sobrino, R. Libonati, J. C. Jiménez-Muñoz, C. C. DaCamara, and M. Romaguera, "Validation of a temperature emissivity separation hybrid method from airborne hyperspectral scanner data and ground measurements in the SEN2FLEX campaign," *Int. J. Remote Sens.*, vol. 29, no. 24, pp. 7251–7268, Dec. 2008.

[39] I. F. Trigo, L. F. Peres, C. C. DaCamara, and S. C. Freitas, "Thermal land surface emissivity retrieved from SEVIRI/Meteosat," *IEEE Trans. Geosci. Remote Sens.*, vol. 46, no. 2, pp. 307–315, Feb. 2008.

[40] G. C. Hulley and S. J. Hook, "Generating consistent land surface temperature and emissivity products between ASTER and MODIS data for earth science research," *IEEE Trans. Geosci. Remote Sens.*, vol. 49, no. 4, pp. 1304–1315, Apr. 2011.

[41] P. Dash, F.-M. Göttsche, and F.-S. Olesen, "Potential of MSG for surface temperature and emissivity estimation: Considerations for real-time applications," *Int. J. Remote Sens.*, vol. 23, no. 20, pp. 4511–4518, Oct. 2002.

Leonardo F. Peres received the B.S. degree in meteorology from the Federal University of Rio de Janeiro, Rio de Janeiro, Brazil, in 1999 and the Ph.D. degree in geophysics from the University of Lisbon, Lisbon, Portugal, in 2005.

Between 2000 and 2005, he was a Research Assistant with the Instituto de Ciência Aplicada e Tecnologia, Lisbon, where he investigated the use of MSG data to retrieve land-surface temperature and emissivity within the framework of the Satellite Application Facility on Land Surface Analysis, which is supported by EUMETSAT. In 2005, he joined the Instituto Nacional de Pesquisas Espaciais, Centro de Previsão de Tempo e Estudos Climáticos, Cachoeira Paulista, SP, Brazil. He was also with the Instituto Dom Luiz, Centro de Geofísica da Universidade de Lisboa, Lisbon. Since 2009, he has been an Assistant Professor with the Department of Meteorology, Federal University of Rio de Janeiro. His current research interests include the retrieval of emissivity and surface temperature from satellite data.

Renata Libonati received the B.S. degree and the Ph.D. degree in geophysics from the University of Lisbon, Lisbon, Portugal, in 2005 and 2011, respectively.

She is currently a Postdoctoral Fellow with the Brazilian National Institute for Space Research (INPE), Sao Jose dos Campos, Brazil. She is also with the Instituto Dom Luiz, Centro de Geofísica da Universidade de Lisboa, Lisbon. Her current research interests include the development and validation of remote sensing algorithms for burned area mapping at regional and global scales.

Carlos C. DaCamara received the Ph.D. degree in atmospheric science from the University of Missouri, Columbia, MO, USA, in 1991.

He is currently an Associate Professor with the Faculty of Sciences, University of Lisbon, Lisbon, Portugal, and is part of the research team of the Instituto Dom Luiz of the University of Lisbon. From May 2003 to April 2004, he was the Vice President of the Instituto de Meteorologia, the Portuguese national meteorological service. Since its beginning in 1999 and until December 2005, he was the Scientific Coordinator of the Land Surface Analysis Satellite Application Facility, an R&D project supported by EUMETSAT. He has been doing research in climatic variability and climate change, namely, with respect to exploring relationships between atmospheric circulation types and large fire events.